Surface mobility of amorphous indomethacin containing moisture and surfactant: A concentration-temperature superposition principle

Yuhui Li, 1 Junguang Yu, 1 Xiao Tan, 1 Lian Yu1*

¹ School of Pharmacy, University of Wisconsin-Madison, Madison, WI, 53705, USA

Abstract

An amorphous material can have vastly higher mobility on the surface than in the bulk and shows fast surface crystallization as a result. Most amorphous materials contain multiple components, but the effect of composition on surface dynamics remains poorly understood. In this study, the surface mobility of amorphous indomethacin was measured using the method of surface grating decay in the presence of moisture and the surfactant Tween 20. It is found that both components significantly enhance the surface mobility, and their effects are well described by the principle of concentration-temperature superposition (CTS); that is, the same surface dynamics is observed at the same T_g -normalized temperature T/T_g , where T_g the composition-dependent glass transition temperature. For systems showing CTS, the mechanism of surface evolution transitions from viscous flow at high temperatures to surface diffusion at low temperatures at 1.04 $T_{\rm g}$. For the surfactant-doped system, the T_g used is the value for the surface layer to account for the surface enrichment of the surfactant (measured by X-ray Photoelectron Spectroscopy). At high surfactant concentration (> 10 % by weight), the surface-grating decay rate in the surface diffusion regime is limited by the large, slow diffusing surfactant molecules; in this case, CTS holds only for the viscous flow regime. The CTS principle allows the prediction of the surface dynamics of multicomponent amorphous materials.

Introduction

There has been significant progress in developing amorphous pharmaceutical formulations to enhance solubility and bioavailability over the traditional crystalline formulations. ¹ It is recognized that the free surface of an amorphous drug can have vastly higher mobility than the bulk, ^{2,3} leading to fast surface crystallization ^{4,5} and eliminating the advantage of the amorphous drug over its crystalline counterpart. In the first measurement of surface diffusion in an amorphous drug, Zhu et al. used the method of surface grating decay and showed that surface diffusion in amorphous indomethacin (IMC) is one million times faster than bulk diffusion at the glass transition temperature T_g . ⁶ Later work investigated the surface diffusion in other amorphous drugs, including nifedipine, ⁷ griseofulvin, ⁸ posaconazole, ³ and itraconazole. ³ In all the amorphous drugs studied to date, surface diffusion is enhanced over bulk diffusion by 4 to 8 orders of magnitude when compared at T_g and shows strong correlation with surface crystal growth. ⁸

Previous studies of the surface mobility of amorphous drugs have focused on pure drugs. An amorphous formulation, however, usually contains other components such as a dispersion polymer and a surfactant. It is important to understand how the other components influence the surface mobility of host molecules. ^{9,10,11} Apart from functional excipients, moisture is often present in a formulation, either taken up from the environment or left over from the manufacturing process. In this work, we investigate the effect of moisture and the surfactant Tween 20 on the surface dynamics of amorphous IMC; see Scheme 1 for the structures of IMC and Tween 20. Moisture is known to enhance the molecular mobility in amorphous formulations and accelerate physical ^{12,13,14,15} and chemical ^{17,18} transformations. Surfactants in amorphous formulations help improve the wetting and dissolution of hydrophobic drugs ^{19,20} and lower the processing

temperature of melt extrusion. ²¹ As generally liquids under ambient conditions, pharmaceutical surfactants can accelerate the molecular mobility and crystallization of amorphous drugs. ^{22,23} Given their similar mobility-enhancing effects, we investigate moisture and the surfactant Tween 20 together in this work.

Scheme 1. Molecular structures of indomethacin and Tween 20

We find that moisture and Tween 20 significantly increase the surface mobility of amorphous IMC. For both dopants, the effects are well described by the principle of *concentration-temperature* superposition (CTS); that is, the same surface dynamics is observed at the same temperature relative to the composition-dependent glass transition temperature $T_{\rm g}$. The mechanism of surface evolution changes from viscous flow at high fluidity (high dopant concentration and high temperature) to surface diffusion at low fluidity, and the transition occurs around $T = 1.04~T_{\rm g}$ for both pure and doped IMC. For Tween 20, the $T_{\rm g}$ used refers to that of the surface layer where the surfactant accumulates. At a high Tween 20 concentration (> 10 %), the slow diffusing dopant molecules limit the surface evolution in the surface-diffusion regime and CTS holds only for the viscous flow regime. According to the CTS, the effect of a dopant on surface mobility can be understood as a first approximation from the shift of $T_{\rm g}$. This result is relevant for predicting the surface mobility of multi-component amorphous formulations.

Materials and Methods

Indomethacin (IMC, purity > 99%) was purchased from Sigma-Aldrich and Tween 20 from EMD Millipore Corporation. Both were used as received. IMC/Tween 20 mixtures were prepared by cryomilling (SPEX CertiPrep 6750) with liquid nitrogen as coolant. Each mixture (1 g) was milled at 10 Hz for 5 cycles, each lasting 2 minutes with a 2-minute cooldown between cycles.

Differential scanning calorimetry (DSC) was performed with a TA Instrument Q2000 unit equipped with a refrigerated cooler. About 5 mg of material was weighed into an aluminum pan and analyzed under 50 mL/min N_2 purge. T_g was determined as the onset of the glass transition during 10 K/min heating.

To make a surface grating, a master pattern was placed on a viscous liquid of IMC (pure or doped) at $T_g + 40$ K and peeled off after vitrification at $T_g - 20$ K. This yielded a glass film with a sinusoidal surface contour. Master gratings of different wavelengths were obtained as follows: for $\lambda = 1000$ nm and 1984 nm, plastic gratings purchased from Rainbow Symphony were used; for $\lambda = 729$ nm and 1478 nm, the masters were duplicated from a DVD or CD, respectively, through a UV-curing polymer (Norland Optical Adhesive 61); for $\lambda = 553$ nm, 3322 nm or 8248 nm, the masters were duplicated from a glass grating (Spectrum Scientific) through the same transfer polymer. All

masters were coated with 10 nm gold before use (Sputter deposition system, Leica ACE600). The thickness of each embossed glass film was 50-100 µm, much larger than the wavelength of any surface grating used, ensuring that the evolution of the top surface was unaffected by the substrate.

The flattening of a surface grating over time was monitored by Atomic Force Microscopy (AFM, Bruker Veeco Multiple Mode IV), laser diffraction, or optical microscopy (Nikon Optiphot 2). AFM was performed in the tapping mode at room temperature; the height profile was Fourier transformed to obtain the amplitude of the sinusoidal surface. Laser diffraction was used to determine faster decay than feasible with AFM. A HeNe laser (λ = 632.8 nm, Uniphase Corp.) passed through a sample film perpendicularly and the first-order diffraction in transmission was recorded with a silicon amplified detector (Thorlabs) interfacing with a National Instruments LabVIEW program. The grating amplitude was verified to be proportional to the square root of diffraction intensity. For long measurements at temperatures below the room temperature, an optical microscope was placed in a walk-in cold room and used to record the diffraction pattern of the surface grating through a Bertrand lens. The incident light was 530 nm obtained by filtering white light with a 20 nm band-pass filter. The sample temperature was controlled with a Linkam microscopic temperature stage or a custom-made mini-oven. The three methods yielded identical results within experimental error when applied to the same decay process.

For control of environmental humidity, nitrogen purge was used to obtain the dry condition (0 % RH) and saturated salt solutions to obtain elevated humidity: Potassium Acetate (21% RH), Potassium Carbonate (43%), Magnesium Nitrate (51%), Potassium Iodide (67%), Sodium Chloride (75%), Potassium Chloride (84%), Potassium Nitrate (92%). For AFM measurements, each surface grating sample was stored in a sealed container of constant RH and removed periodically for analysis. For laser diffraction measurements, a saturated salt solution was placed in the custom-built temperature stage and sealed with the sample (see the inset of Figure 2a).

X-ray Photoelectron Spectroscopy (XPS) was performed with a Thermo Scientific K-alpha equipped with an Al K α X-ray source (1486.6 eV). XPS was used to determine the surface compositions of amorphous IMC/Tween 20 films. Each film was prepared by melting a mixture of interest, annealing at 343 K for 1 min, and quenching to room temperature by contact with an

aluminum block. The films were kept in a desiccator before measurements. The X-ray spot size was 400 μm. The pass energy was 200 eV (1 eV step resolution) for survey scans and 50 eV (0.1 eV step resolution) for high-resolution scans. The XPS data were analyzed using the Avantage software (Thermo Scientific) and the Cl 2p peak at 200.2 eV of benzyl chloride was used to calibrate the binding energy. The peak area of each element was converted to its surface atomic composition using the Relative Sentivity Factor. ²⁵ The mass fraction of Tween 20 at the free surface was calculated as follows:

$$w_{T20} = \frac{(4 x_{Cl/O} - 1) \cdot M_{T20}}{(4 x_{Cl/O} - 1) \cdot M_{T20} - 26 x_{Cl/O} \cdot M_{IMC}}$$
(1)

where $x_{\text{CI/O}}$ is the ratio of the Cl and O peaks, M_{IMC} and M_{T20} are the molecular weights of IMC and Tween 20, and the factors 4 and 26 are the numbers of oxygen atoms in each IMC and Tween 20 molecule, respectively.

Results and Discussion

Both dopants investigated in this work, water and Tween 20, enhance the *bulk* mobility of amorphous IMC. Figure 1a shows the DSC traces of IMC doped with Tween 20. Each mixture exhibits a single glass transition temperature (T_g) whose value decreases with increasing Tween 20 concentration. These results indicate that IMC and Tween 20 are miscible in the range of concentration tested. ²⁶ Figure 1b plots the T_g of the mixture against the concentration of Tween 20 as well as the literature data on water. ²⁷ For both dopants, the effect on IMC T_g is well fitted by the Gordon-Taylor equation: ²⁸

$$T_{g mix} = \frac{w_1 T_{g_1} + k w_2 T_{g_2}}{w_1 + k w_2} \tag{2}$$

Where w_1 is the weight fraction of water or Tween 20, w_2 is the weight fraction of IMC, T_{g1} is the T_g of water (135 K)²⁷ or Tween 20 (208 K,

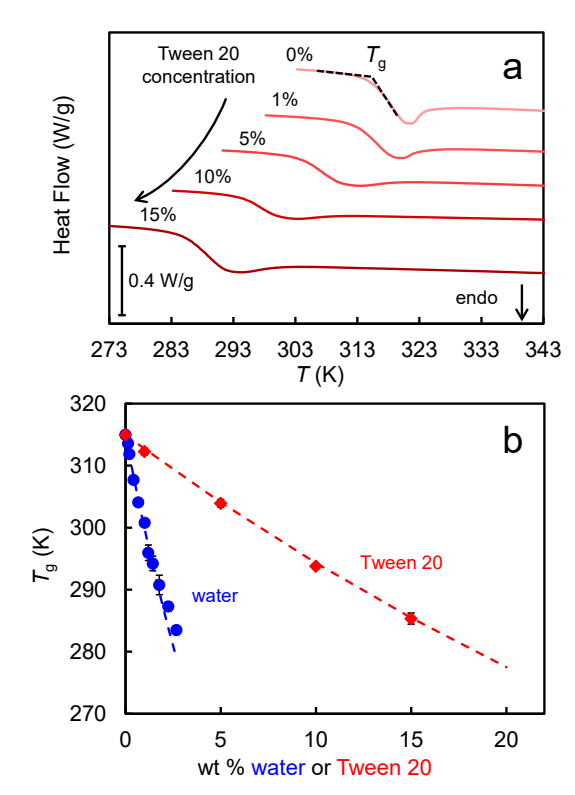


Figure 1. (a) DSC traces of Tween 20/IMC mixture for T_g . (b) T_g vs. the concentration of water²⁷ or Tween 20 in IMC. The dashed lines are fits to the Gordon-Taylor equation.

measured by DSC in this work), T_{g2} is the T_g of IMC (315 K), and k is a model parameter treated here as a fitting constant. For water as the second component, k = 0.11, and for Tween 20, k = 0.46.

Effect of Moisture on IMC Surface Mobility.

Figure 2 shows the typical surface grating decay curves. For a laser-diffraction measurement (Figure 2a), a homemade sample cell was used to maintain the temperature and humidity of the sample (see the drawing in the inset). The headspace between the sample and the saturatedsalt solution was minimized to ensure rapid equilibration of humidity. The intensity of the first-order diffraction peak I was found to decrease exponentially over time. For an AFM measurement (Figure 2b), the amplitude of the sinusoidal surface grating, h, was measured as a function of time and is seen to decrease exponentially. Considering the fact that $I \propto h^2$, the decay curves were fitted to the function, I = $I_0 \exp(-2Kt)$ for the diffraction data and $h = h_0$ $\exp(-Kt)$ for the AFM data, where K is the decay constant.

Figure 3 shows the decay curves of a 1000 nm wavelength IMC surface grating at different RH at 298 K and 303 K. With increasing RH, the

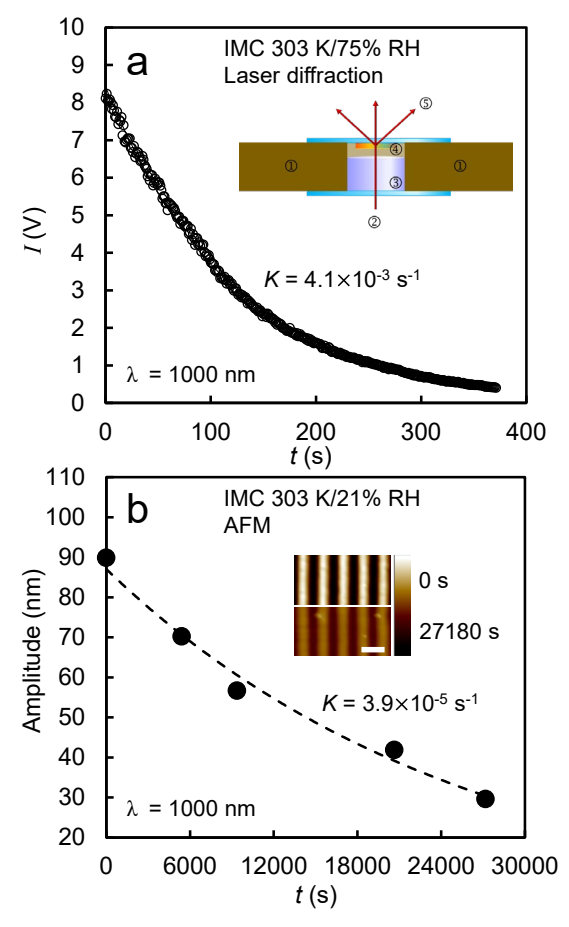


Figure 2. (a) IMC surface grating decay at 303 K and 75 % RH measured by laser diffraction. Inset: experimental setup. ①Copper block for temperature control. ②Laser. ③Saturated salt solution for humidity control. ④Surface grating. ⑤First-order diffraction. (b) IMC surface grating decay at 303 K and 21 % RH measured by AFM. Inset: AFM images at two time points. REMOVE COLOR SCALE. The scale bar corresponds to 1 μm in length.

decay rate significantly increases. At 298 K, it took two days for the grating amplitude to decrease 50 % under the dry condition, while it only took several minutes at 92 % RH. The curves running through the data points are the exponential fits, from which we obtain the surface-grating decay

constant *K*. In Figure 3c, *K* is plotted against RH at 298 K and 303 K. From 0 to 92 % RH, *K* increases by roughly 4 orders of magnitude at each temperature. The decay constant shows a stronger dependence on RH at higher RH values and this reflects a change of surface-evolution mechanism (see below).

According to Mullins, a sinusoidal surface grating decays exponentially with a decay constant K given by:²⁹

$$K = Fq + Aq^2 + (A' + C)q^3 + Bq^4$$
 (3)

where $q = 2\pi/\lambda$ is the spatial frequency of the grating with λ being the grating wavelength and the different terms correspond to the different mechanisms of surface evolution: viscous flow (F), evaporation-condensation (A and A'), bulk diffusion (C), and surface diffusion (B). For amorphous materials, viscous flow and surface diffusion are often found to be the two leading mechanisms, 3 with viscous flow being the collective movement of a liquid and surface diffusion the migration of individual atoms or molecules in the surface layer. For each decay mechanism, the decay rate has a characteristic

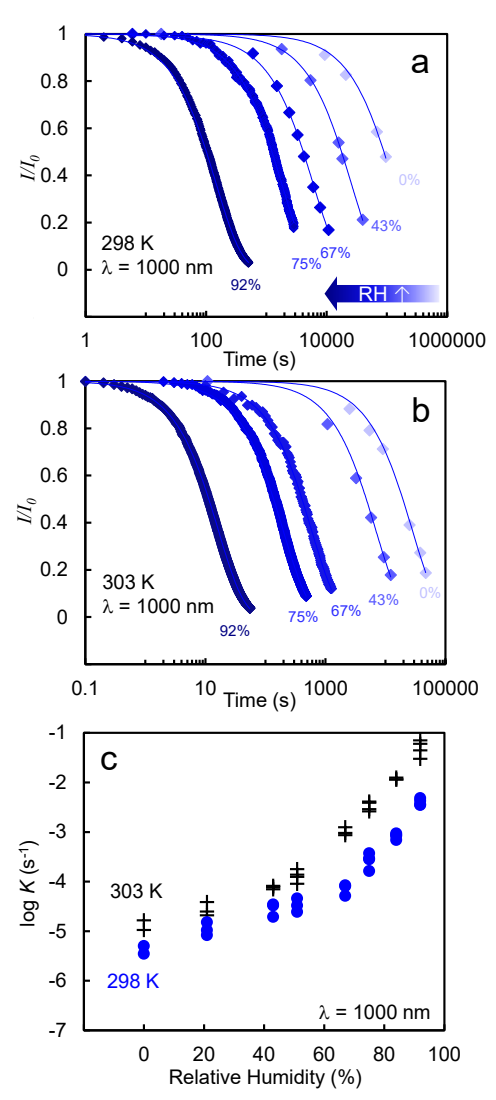


Figure 3. (a) Decay curves at 298 K and different RH. (b) Decay curves at 303 K and different RH. The solid lines are exponential fits. (c) Humidity dependence of the decay constant, *K*, for IMC surface gratings at 303 K and 298 K.

dependence on the grating wavelength; for example, $K \propto \lambda^{-1}$ for viscous flow and $K \propto \lambda^{-4}$ for surface diffusion. This is the basis for a wavelength test of the decay mechanism. By this test, Zhu et al. showed that for pure IMC, viscous flow and surface diffusion are the dominant mechanisms for surface evolution⁶ and we apply the same test to the binary systems of this study.

Figure 4a shows the wavelength dependence of the decay constant K for IMC at 303 K and different RH. At 75 % RH, K is proportional to λ^{-1} , consistent with the viscous flow mechanism, whereas at 0 % RH and 21% RH, a stronger wavelength dependence is observed, $K \propto \lambda^{-4}$, indicating the surface diffusion mechanism. This transition of the surface-evolution mechanism is confirmed by the exposure of nanoparticles during grating decay. Ruan et al. showed that despite its high chemical purity, indomethacin contains trace amount of nanoparticles and these nanoparticles can be exposed or remain embedded depending on the mechanism of surface evolution. 30 If the mechanism is viscous relaxation, the particles flow with the liquid and remain embedded; however, if the mechanism is surface diffusion, they become exposed as the fast-diffusing IMC molecules vacate the peaks of the surface grating for the valleys. Figure 4b shows the AFM images of the surface gratings after partial decay from the initial amplitude of 100 nm to 30 nm at four RH levels at 303 K. Nanoparticles are exposed during decay at 0 % RH and 21 % RH, but not observed at high 67 % RH; at 51% RH, we observe an intermediate behavior with hints of particle exposure. These results are in agreement with the change of the surface-evolution mechanism concluded above.

In Figure 5, the surface grating decay constant is plotted against the T_g -normalized temperature. The

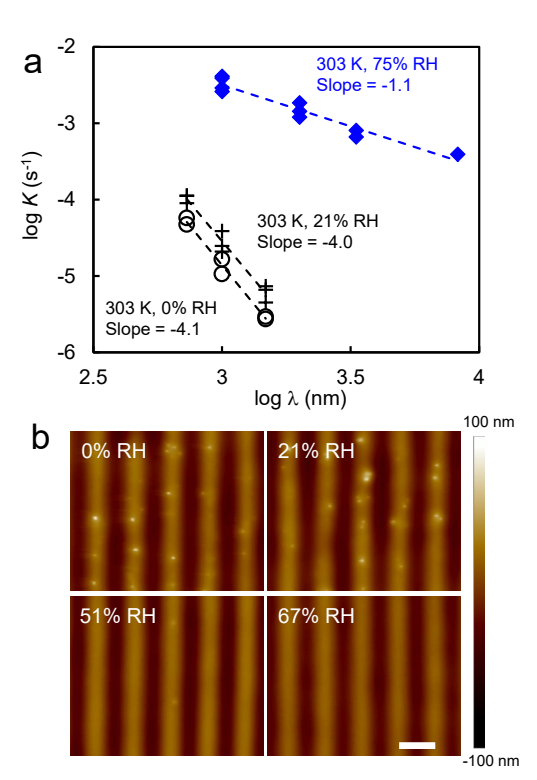


Figure 4. (a) Wavelength dependence of IMC at different humidity levels at 303 K. (b) AFM images of IMC surface gratings at 303 K at different RH. The initial grating amplitude was 100 nm and the samples were observed after the amplitudes decayed to 30 nm. The scale bar corresponds to 1 μm. The color scale indicates surface height.

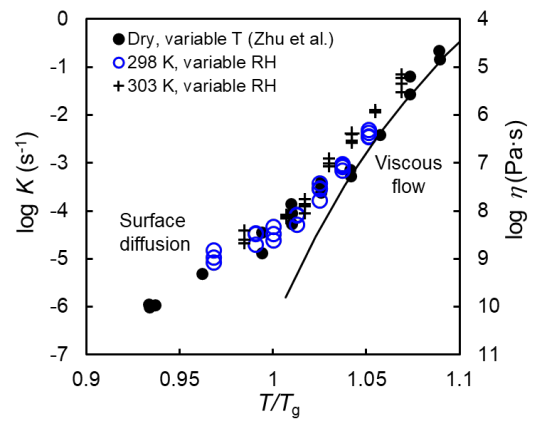


Figure 5. Surface grating decay constants of dry and moist IMC as a function of T/T_g , where T_g is the composition-dependent glass transition temperature. The solid curve is the viscosity of IMC under dry condition.

black open circles correspond to dry IMC at different temperatures;⁶ the other symbols correspond to moist IMC at different RH at 298 and 303 K. In this format, the data points approximately collapse to a common trend regardless of whether they were measured as a function of RH at a fixed temperature or as a function of temperature under a dry condition. Also plotted in Figure 5 is the viscosity of pure IMC³¹ using the second y axis. At high fluidity (high T/T_g), the decay constants K track the viscosity, $K \propto \eta^{-1}$, confirming the assignment of the surface-evolution mechanism as viscous flow. At low fluidity (low T/T_g), the decay is faster than the viscosity trend, indicating a change of the surface-evolution mechanism with the new decay mechanism being surface diffusion by the wavelength test (Figure 4a).

This data collapse seen in Figure 5 means that the surface grating of water-containing IMC decays at approximately the same rate as that of dry IMC if the comparison is made at the same temperature normalized by $T_{\rm g}$. We call this result Concentration-Temperature Superposition (CTS), in analogy to Time-Temperature Superposition (TTS) in polymer dynamics, ³² Rate-Temperature Superposition (RTS) in vapor deposition, ³³ and Time-Water Superposition in describing the effect of water on polymer dynamics. ^{34,35} According to CTS, the effect of moisture on surface dynamics can be understood on the basis of the temperature effect on surface dynamics in the dry material and a decrease of $T_{\rm g}$ by water absorption. For both dry and moist IMC, surface evolution occurs by viscous flow at high fluidity and by surface diffusion at low fluidity, with the transition occurring near T = 1.04 $T_{\rm g}$ for the 1000 nm wavelength surface grating. This principle is potentially useful for predicting the effect of a second component on surface mobility and we show below that it is also valid for a surfactant as a second component.

Effect of Surfactant Tween 20 on IMC Surface Mobility.

Figure 6a shows the typical data on the effect of Tween 20 on IMC surface mobility. Here we compare IMC containing Tween 20 at different concentrations at 303 K. As the Tween 20 concentration increases, the surface grating flattens at a faster rate. For these samples, the time required to flatten the grating decreases from one day for pure IMC to 10 seconds if 15 % Tween 20 is present. The curves through the data points are the exponential fits, from which we obtain the decay constants K.

In Figure 6b, the decay constants of IMC containing Tween 20 are plotted against temperature. For comparison, we also plot the decay rate of pure IMC⁶ and its bulk viscosity. The doping of Tween 20 greatly accelerates the surface grating decay. Note that at 1 % or 5 % Tween 20, the K vs. temperature plot shows a kink, as seen with pure IMC. This suggests a change of the mechanism of surface evolution. To investigate this, a wavelength test similar to that in Figure 4a was performed for the 5 % sample and the result is shown in Figure 7. This test established that the decay mechanism is viscous flow at a high temperature (318 K) and surface diffusion at a low temperature (298 K).

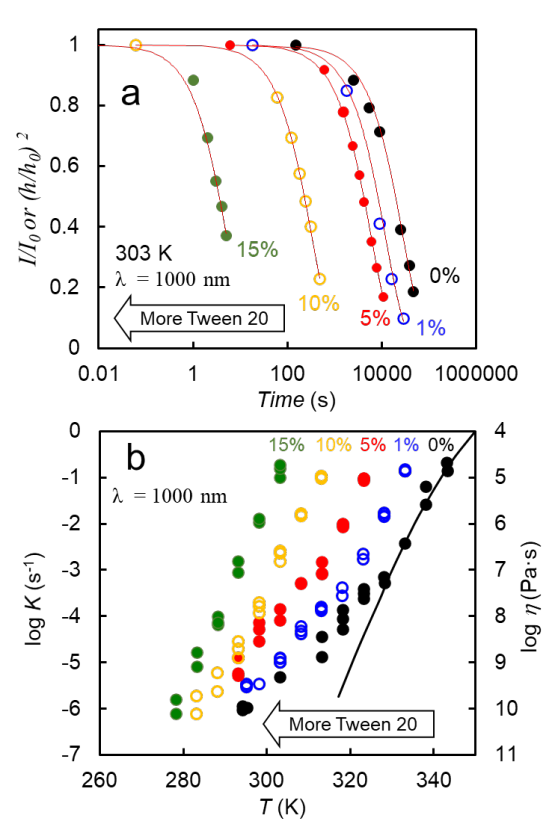


Figure 6. (a) Surface-grating decay kinetics of IMC containing Tween 20 at 303 K. The solid lines are the exponential fits. (b) Decay constant *K* vs. temperature for IMC containing Tween 20.

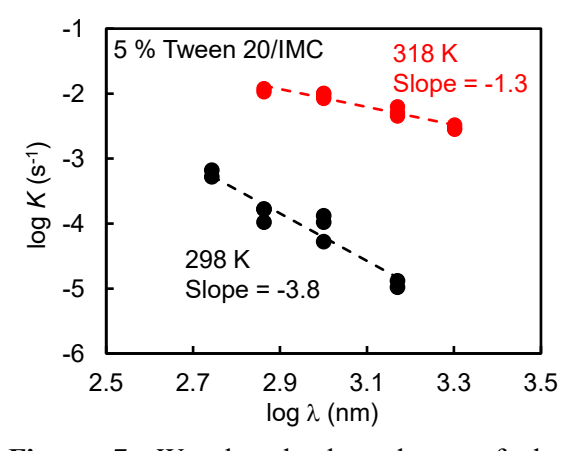


Figure 7. Wavelength dependence of the surface-grating decay constant K for IMC containing 5 % Tween 20 at 298 K and 318 K.

At 15 % Tween 20, there is no obvious kink in the K vs T curve and the decay mechanism is presumably viscous flow at all the temperatures investigated. At 10 % Tween 20, there is a weak hint of a kink, possibly indicating a transition to surface diffusion at low temperatures.

To test the validity of CTS in describing the IMC/surfactant system, in Figure 8a, we plot the surface-grating decay constants K against T/T_g as in Figure 5. We observe a significant collapse of data points, while the quality of the collapse is slightly worse than that of Figure 5. At high T/T_g , the data points for the surfactant-containing samples show a good master curve, but they lie above the points for pure IMC by approximately one order of magnitude. This suggests that Tween 20 has a larger effect on the mobility at the free surface than it does in the bulk. Furthermore, the surfactant-containing samples do not form a master curve at low T/T_g : the lighter-doped samples (1 and 5 %) roughly join the points for pure IMC, but the heavier-doped samples (10 and 15 %) have significantly lower values. This is attributed to the slow surface diffusion rate of surfactant and will be addressed later.

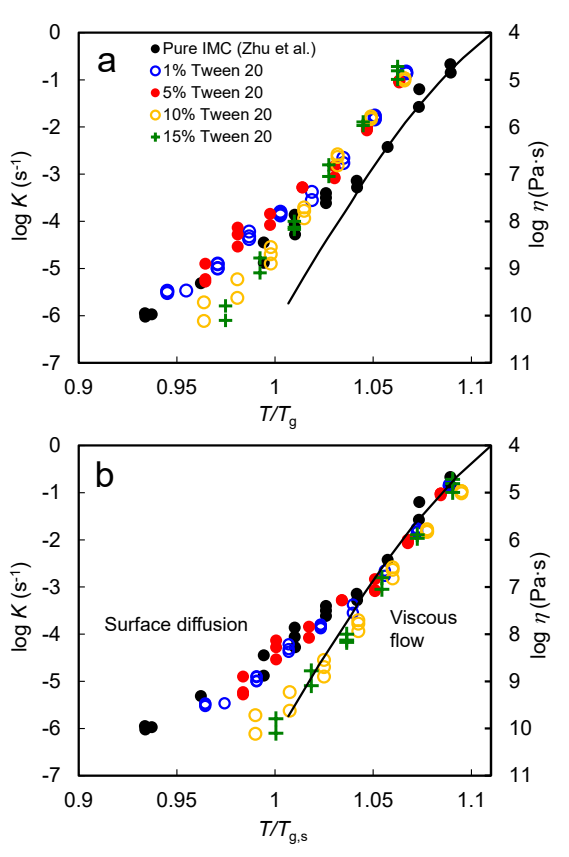


Figure 8. Surface-grating decay constant of IMC containing Tween 20 as a function of T/T_g , where T_g is the composition-dependent bulk glass transition temperature (a) or the surface glass transition temperature $T_{g,s}$ after correction for the surface enrichment of Tween 20.

Given that a surfactant can preferentially enrich at the surface of an amorphous drug, ³⁶ we investigated whether this effect occurs in Tween 20 doped IMC and thus leads to the imperfect data collapse in Figure 8a. Surfactants are known to enrich at the air/water interface and Yu et al. reported recently that the same can occur at the free surface of the amorphous drugs. We measured the surface concentration of Tween 20 using XPS. ^{37,38} Figure 9 shows the spectra of Cl 2p and O 1s in our samples. With increasing Tween 20 concentration, the Cl peak decreases and the O peak

increases. From these results, the surface concentrations of Tween 20 were calculated (eq. 1) and the results are given in Table I and plotted in Figure 9c.

Figure 9c shows that the surface concentration of Tween 20 is systematically higher than its bulk concentration. This finding is consistent with the recent report on other drug-surfactant systems.36 Given that Tween 20 plasticizes IMC (Figure 1), its enrichment on the surface means that the surface $T_{\rm g}$ is lower than the bulk $T_{\rm g}$. To calculate the surface $T_{\rm g}$ of IMC containing Tween 20, we assume that the same plasticizing effect in the bulk (Figure 1b) occurs in the surface region. The calculation was performed using eq. 2, whose parameters were obtained by fitting the bulk data. The results of this calculation are shown in Table I. According to this calculation, the surface T_g is 6-8 K below the bulk T_g . This effect qualitatively explains why in Figure 8a the surfactant-doped samples as a group show faster surface dynamics relative to pure IMC.

For a quantitative test of our conclusion, in Figure 8b, we replot the data in Figure 8a using the surface glass transition temperature $T_{\rm g,s}$ as the normalizing temperature. We observe significantly improved data collapse. The overall pattern is similar to that for water-containing IMC (Figure 5). At high fluidity (high $T/T_{\rm g}$), the decay constants K track the viscosity, $K \propto \eta^{-1}$, confirming viscous flow as the surface-evolution mechanism. At low fluidity (low $T/T_{\rm g}$), the two lighter-

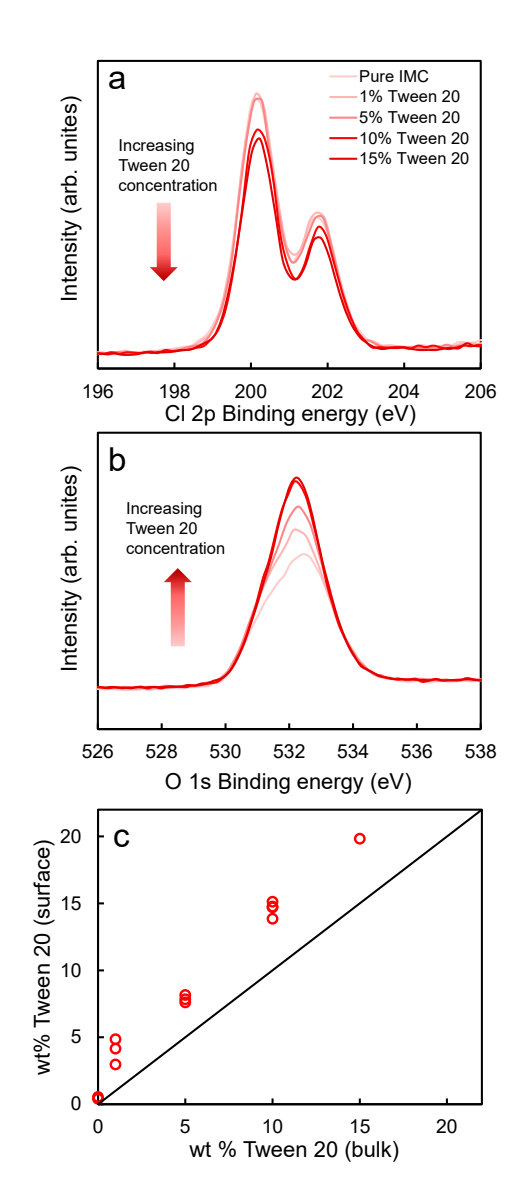


Figure 9. XPS spectra of Cl 2p (a) and O 1s (b) of IMC containing Tween 20 at concentrations indicated. (c) Surface concentration of Tween 20 vs. bulk concentration. The surface concentration is higher than the bulk concentration; the diagonal line indicates the condition that the two concentrations are equal.

doped mixtures (1 and 5 %) join the trend of pure IMC; their decay rates are faster than the viscosity trend, indicating a new mechanism for surface evolution. The transition occurs near $T = \frac{1}{2} \int_{-\infty}^{\infty} \frac{1}{2} \int_$

1.04 T_g and the new mechanism was determined to be surface diffusion by the wavelength test (Figure 7). For these lighter-doped mixtures, we observe a collapse of data points with pure IMC; that is, the systems follow CTS.

For the two heavier-doped mixtures (10 and 15 %), the deviation from the viscosity trend at low fluidity is less pronounced. This indicates that surface diffusion is slower in these systems, allowing viscous flow to dominate surface evolution down to lower temperatures. These two systems do not follow the CTS behavior of IMC containing water and IMC containing Tween 20 at low concentrations.

The inhibitory effect of Tween 20 on the surface diffusion in amorphous IMC is analogous to the observation of Zhang et al. They reported that 1 % of polystyrene (PS) by weight in amorphous oterphenyl (OTP) has little effect on the rate of surface-grating decay in the viscous-flow regime, but a significant inhibitory effect in the surface-diffusion regime. They explained the effect as follows: in the viscous-flow regime, PS and OTP flow together, whereas in the surface-diffusion regime, the faster-diffusing OTP vacates the peaks of a surface grating while the slower diffusing PS is stranded behind, resulting in a slower apparent decay rate. The same explanation appears to apply to Tween 20 doped IMC. Tween 20 is a larger molecule than IMC with a molecular weight of 1227.5 g/mol to IMC's 357.8 g/mol, and it could be strongly oriented in the surface layer as a surfactant. 39,40 These let surface Tween 20 molecules have a deeper penetration into the bulk and slower surface diffusion than IMC molecules.^{2,41,42} At low concentrations (1 and 5 %), our results indicate that the Tween 20 molecules can flow and surface-diffuse with the IMC molecules, resulting in the master-curve behavior in Figure 8b. At high concentrations (10 and 15 %), the inhibitory effect of Tween 20 becomes noticeable in the surface-diffusion regime, where the slowdiffusing molecules are stranded in the surface regions vacated by IMC, causing a slow surfacegrating decay. With water as the dopant, the complexity described above for PS9 and Tween 20 does not arise. Water is a faster diffuser than the IMC host molecules; in the viscous-flow regime, water flows with the host molecules; in the surface-diffusion regime, water never gets stranded in the regions vacated by the host molecules. As a result, the IMC-water mixtures show CTS in the entire concentration range.

Table I. Bulk and surface concentrations of Tween 20 and $T_{\rm g}$

bulk %	Bulk Cl/O	surface Cl/O	surface %	$T_{\rm g},{ m K}$	$T_{g,s}$, K
0	0.250	-	-	315	-
1	0.245	0.231 (0.0042)	3.99 (0.95)	312	306
5	0.227	0.215 (0.0012)	7.87 (0.28)	304	298
10	0.207	0.188 (0.0020)	14.6 (0.53)	294	286
15	0.187	0.171 (0.0004)	19.8 (0.11)	285	278

In each parenthesis is the standard deviation calculated from three measurements of the same sample.

In Figure 10, we plot the data on the two dopants (moisture and Tween 20) together. For the Tween 20 systems, only the two lighter-doped mixtures (1 and 5 %) are plotted. We observe a reasonably good data collapse for all the systems. They all show a similar transition from the viscous flow regime to the surface-diffusion regime with the transition temperature near 1.04 T_g and the transition viscosity approximately 10^7 Pa s.

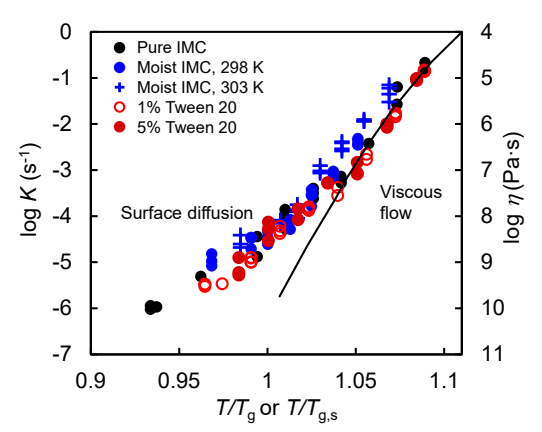


Figure 10. Grating decay constants of pure or doped IMC as a function of temperature.

Conclusion

This study has found that moisture and the surfactant Tween 20 can significantly accelerate the surface mobility of amorphous indomethacin. The magnitude of the acceleration is well described by the principle of Concentration-Temperature Superposition (CTS). According to CTS, the same surface dynamics is observed at the same temperature relative to the composition-dependent glass transition temperature $T_{\rm g}$. The evolution mechanism changes from viscous flow at high fluidity to surface diffusion at low fluidity with the transition occurring near 1.04 $T_{\rm g}$ for both pure and doped IMC. For Tween 20, CTS is observed after taking into account its surface enrichment effect characterized by XPS. In the high-temperature region where viscous flow dominates surface evolution, CTS holds for all the systems, whereas in the low-temperature region where surface

diffusion dominates surface evolution, CTS is observed for IMC containing moisture at any concentration and for Tween 20 at lower concentrations (1 and 5 %). At higher Tween 20 concentrations, we observe deviation from CTS and attribute the effect to the large difference between the surface diffusion rates of the guest and host molecules. We anticipate that CTS can be used for predicting surface mobility in multi-component amorphous materials. Given that fast surface dynamics enables fast crystal growth at the free surface of amorphous drugs, the two dopants investigated here, water and surfactant, are expected to accelerate the surface crystallization process. It is of interest to learn whether the previously observed correlation between the surface diffusion coefficient and the surface crystal growth rate for pure systems still holds for binary systems. If so, CTS could be extended to predict crystal growth rates in multi-component amorphous formulations. Given the high degree of surface enrichment observed in some drug-surfactant systems, it is of interest to learn whether CTS holds under such extreme conditions.

Conflicts of interest

There are no conflicts of interest to declare.

Acknowledgements

This research was primarily supported by NSF through the University of Wisconsin Materials Research Science and Engineering Center (Grant DMR-1720415). JY and LY thank the support from Bristol Myers Squibb.

References

¹ Yu, L. Amorphous Pharmaceutical Solids: Preparation, Characterization and Stabilization. *Adv. Drug Deliv. Rev.* **2001,** *48*, 27

² Yu, L. Surface mobility of molecular glasses and its importance in physical stability. *Adv. Drug Deliv. Rev.* **2016**, *100*, 3-9.

³ Li, Y.; Zhang, W.; Bishop, C.; Huang, C.; Ediger, M.D.; Yu, L. Surface diffusion in glasses of rod-like molecules posaconazole and itraconazole: Effect of interfacial molecular alignment and bulk penetration. *Soft. Matt.* **2020**, *16*, 5062-5070.

⁴ Sun, Y.; Zhu, L.; Kearns, K. L.; Ediger, M.D.; Yu, L. Glasses crystallize rapidly at free surfaces by growing crystals upward. *Proc. Natl. Acad. Sci.* **2011**, *108*, 5990

⁵ Wu, T.; Yu, L. Surface crystallization of indomethacin below Tg. *Pharm. Res.* **2006**, *23*, 2350

⁶ Zhu, L.; Brian, C. W.; Swallen, S. F.; Straus, P. T.; Ediger, M. D.; Yu, L. Surface self-diffusion of an organic glass. *Phys. Rev. Lett.* **2011**, *106*(25), 256103.

⁷ Brian, C. W.; Yu, L. Surface Self-Diffusion of Organic Glasses. *J. Phys. Chem. A.* **2013**, *117*, 13303–13309.

- ⁸ Huang, C., Ruan, S., Cai, T., Yu, L. Fast surface diffusion and crystallization of amorphous griseofulvin. *J. Phys. Chem. B* **2017**, *121*(40), 9463-9468.
- ⁹ Zhang, W.; Teerakapibal, R.; Yu, L. Surface mobility of amorphous o-terphenyl: a strong inhibitory effect of low-concentration polystyrene. *J. Phys. Chem. B* **2016**, *120*(27), 6842-6847.
- ¹⁰ Bannow, J.; Karl, M.; Larsen, P. E.; Hwu, E. T.; Rades, T. Direct Measurement of Lateral Molecular Diffusivity on the Surface of Supersaturated Amorphous Solid Dispersions by Atomic Force Microscopy. *Mol. Pharm.* **2020**, *17*(5), 1715-1722.
- ¹¹ Liu, J.; Hwu, E.T.; Bannow, J.; Grohganz, H.; Rades, T. Impact of Molecular Surface Diffusion on the Physical Stability of Co-Amorphous Systems. *Mol. Pharm.* **2022**, *19*, 1183–1190
- ¹² Miyazaki, T.; Yoshioka, S.; Aso, Y.; Kawanishi, T. Crystallization rate of amorphous nifedipine analogues unrelated to the glass transition temperature. *Int. J. Pharm.* **2007**, *336*(1), 191-195.
- ¹³ Greco, S.; Authelin, J. R.; Leveder, C.; Segalini, A. A practical method to predict physical stability of amorphous solid dispersions. *Pharm. Res.* **2012**, *29*(10), 2792-2805.
- ¹⁴ Mehta, M.; Kothari, K.; Ragoonanan, V.; Suryanarayanan, R. Effect of water on molecular mobility and physical stability of amorphous pharmaceuticals. *Mol. Pharm.* **2016**, *13*(4), 1339-1346.
- ¹⁵ Mehta, M.; Suryanarayanan, R. Accelerated physical stability testing of amorphous dispersions. *Mol. Pharm.* **2016**, *13*(8), 2661-2666.
- ¹⁶ Purohit, H. S.; Ormes, J. D.; Saboo, S.; Su, Y.; Lamm, M. S.; Mann, A. K.; Taylor, L. S. Insights into nanoand micron-scale phase separation in amorphous solid dispersions using fluorescence-based techniques in combination with solid state nuclear magnetic resonance spectroscopy. *Pharm. Res.*, **2017**, *34*(7), 1364-1377.
- ¹⁷ Waterman, K. C.; Carella, A. J.; Gumkowski, M. J.; Lukulay, P.; MacDonald, B. C.; Roy, M. C.; Shamblin, S. L. Improved protocol and data analysis for accelerated shelf-life estimation of solid dosage forms. *Pharm. Res.* **2007**, *24*(4), 780-790.
- ¹⁸ Shalaev, E. Y.; Zografi, G. How does residual water affect the solid-state degradation of drugs in the amorphous state? *J. Pharm. Res.* **1996**, *85*(11), 1137-1141.
- ¹⁹ Saboo, S.; Bapat, P.; Moseson, D. E.; Kestur, U. S.; Taylor, L. S. Exploring the Role of Surfactants in Enhancing Drug Release from Amorphous Solid Dispersions at Higher Drug Loadings. *Pharmaceutics*, **2021**, *13*(5), 735.
- ²⁰ Sekhon, B. S. Surfactants: pharmaceutical and medicinal aspects. *J. Pharm. Technol. Res. Manag.* **2014** , *1*(1), 43-68.
- ²¹ Solanki, N. G.; Lam, K.; Tahsin, M.; Gumaste, S. G.; Shah, A. V.; Serajuddin, A. T. Effects of surfactants on itraconazole-HPMCAS solid dispersion prepared by hot-melt extrusion I: miscibility and drug release. *J. Pharm. Sci.* **2019**, *108*(4), 1453-1465.
- ²² Zhang, J.; Shi, Q.; Tao, J.; Peng,Y.; Cai, T. Impact of Polymer Enrichment at the Crystal-Liquid Interface on Crystallization Kinetics of Amorphous Solid Dispersions. *Mol. Pharm.* **2019**, *16*(3), 1385-1396.
- ²³ Mosquera-Giraldo, L. I.; Trasi, N. S.; Taylor, L. S. Impact of surfactants on the crystal growth of amorphous celecoxib. *Int. J. Pharm.* **2014**. *461*(1-2), 251-257.
- ²⁴ Greenspan, L. Humidity fixed points of binary saturated aqueous solutions. *J. Res. Nat. Bur. Stand,* **1977**, *81*(1), 89-96.
- ²⁵ Wagner, C. D.; Davis, L. E.; Zeller, M. V., Taylor, J. A.; Raymond, R. H.; Gale, L. H. Empirical atomic sensitivity factors for quantitative analysis by electron spectroscopy for chemical analysis. *Surf. Interface Anal.* **1981**, *3*(5), 211-225.
- ²⁶ Sun, Y.; Tao, J.; Zhang, G. G. Z.; Yu, L. Solubilities of crystalline drugs in polymers: an improved analytical method and comparison of solubilities of indomethacin and nifedipine in PVP, PVP/VA, and PVAc. *J. Pharm. Sci.* **2010**, 99, 4023–4031.
- ²⁷ Andronis, V.; Yoshioka, M.; Zografi, G. Effects of sorbed water on the crystallization of indomethacin from the amorphous state. *J. Pharm. Sci.* **1997**, *86*(3), 346-351.
- ²⁸ Gordon, M.; Taylor, J. S. Ideal copolymers and the second-order transitions of synthetic rubbers. I. Non-crystalline copolymers. *J. Appl. Chem.* **1952**, *2*(9), 493-500.
- ²⁹ Mullins, W.W. Flattening of a nearly plane solid surface due to capillarity. J. Appl. Phys. **30**, 77 (1959).
- ³⁰ Ruan, S.; Musumeci, D.; Zhang, W.; Gujral, A.; Ediger, M. D.; Yu, L. Surface transport mechanisms in molecular glasses probed by the exposure of nano-particles. *J. Chem. Phys.* **2017**, *146*(20), 203324.

³¹ Andronis, V.; Zografi, G. Molecular mobility of supercooled amorphous indomethacin, determined by dynamic mechanical analysis. *Pharm. Res.* **1997**, *14*(4), 410-414.

- ³² Hiemenz, P. C.; Lodge, T. P. Polymer chemistry. CRC press. 2007
- ³³ Bishop, C.; Gujral, A.; Toney, M. F.; Yu, L.; Ediger, M. D. Vapor-deposited glass structure determined by deposition rate–substrate temperature superposition principle. *J. Chem. Phys. Lett.* **2019**, *10*(13), 3536-3542.
- ³⁴ Zhou, S. M.; Tashiro, K.; Ii, T. Confirmation of universality of time–humidity superposition principle for various water-absorbable polymers through dynamic viscoelastic measurements under controlled conditions of relative humidity and temperature. *J Polym Sci B Polym Phys* **2001**, 39(14), 1638-1650.
- ³⁵ Suarez-Martinez, P. C.; Batys, P.; Sammalkorpi, M.; Lutkenhaus, J. L. Time–temperature and time–water superposition principles applied to poly (allylamine)/poly (acrylic acid) complexes. *Macromolecules*, **2019**, *52*(8), 3066-3074.
- ³⁶ Yu, J.; Li, Y.; Yao, X.; Que, C.; Huang, L.; Hui, H.W.; Gong, Y.C.; Yu, L. Surface Enrichment of Surfactants in Amorphous Drugs: An X-Ray Photoelectron Spectroscopy Study. *Mol. Pharm.*, **2022**, *19*, 654-660
- ³⁷ Wan F.; Bohr, A.; Maltesen M.J.; Bjerregaard S.; Foged C.; Rantanen J. et al. Critical solvent properties affecting the particle formation process and characteristics of celecoxib-loaded PLGA microparticles via spray-drying. *Pharm Res.* **2013**, *30*(4), 1065–76.
- 38 Davies M.C.; Wilding I.R.; Short R.D.; Khan M.A.; Watts J.F.; Melia C.D. An analysis of the surface chemical structure of polymethacrylate (Eudragit) film coating polymers by XPS. *Int. J. Pharm.* **1989**, *57*(3), 183–187.
- ³⁹ Ward, R.; Davies, P.; Bain, C., Orientation of surfactants adsorbed on a hydrophobic surface. *J. Phys. Chem.* **1993**, 97(28), 7141-7143.
- ⁴⁰ Rasing, T.; Shen, Y.; Kim, M. W.; Valint Jr, P.; Bock, J. Orientation of surfactant molecules at a liquidair interface measured by optical second-harmonic generation. *Phys. Rev. A* **1985**, *31*(1), 537.
- ⁴¹ Li, Y.; Bishop, C.; Cui, K.; Schmidt, J. R.; Ediger, M. D.; Yu, L. Surface diffusion of a glassy discotic organic semiconductor and the surface mobility gradient of molecular glasses. *J. Chem. Phys.* **2022**, *156*, 094710
- ⁴² Schweizer, K. S.; Simmons, D. S. Progress towards a phenomenological picture and theoretical understanding of glassy dynamics and vitrification near interfaces and under nanoconfinement. *J. Chem. Phys.* **2019**, *151*, 240901.

${\it C}$ oncentration- ${\it T}$ emperature ${\it S}$ uperposition

